Catal Lett (2008) 121:283–290
DOI 10.1007/s10562-007-9334-z

Pure H_2 Production by Decomposition of Methane Over Ni Supported on Hydroxyapatite Catalysts

J. Ashok · S. Naveen Kumar · M. Subrahmanyam · A. Venugopal

Received: 29 August 2007 / Accepted: 1 November 2007 / Published online: 20 November 2007

Abstract The catalytic decomposition of CH_4 for the production of pure H_2 is carried out over Ni supported on hydroxyapatite [$Ca_5(PO_4)_3(OH)$] catalysts at 650 °C and atmospheric pressure. CH_4 decomposition activity is decreased with time on stream and finally deactivated completely. The physicochemical properties of the fresh catalysts are characterized by XRD, DTA/TG, TPR and SEM techniques along with CHNS analyses of the used samples. It is found that the 30 wt% Ni/HAp displayed higher H_2 production rates over the other Ni loadings, which is correlated with Ni metal surface area measured by O_2 pulse chemisorption.

Keywords Hydroxyapatite · Methane decomposition · Hydrogen production · Carbon filaments · Ni metal area

1 Introduction

Hydrogen is produced from steam reforming, partial oxidation or autothermal reforming of hydrocarbons and alcohols [1]. A drawback in above processes is the formation of CO, which is difficult to separate from hydrogen. Thus produced hydrogen can be used in fuel cells, provided the carbon monoxide is removed completely from hydrogen streams or reduce the levels down to 10 ppm in order to prevent the poisoning of platinum electrode in fuel cell. The direct catalytic cracking of hydrocarbons especially methane into hydrogen and carbon is an attractive alternative method due to growing importance on the production of pure H_2 as well as the formation of useful compounds such as carbon nanotubes (CNT) and carbon nanofibers (CNF) [2–6] thus the catalytic decomposition of methane (CDM) has become a topical subject [7–13].

Nickel is a common transition metal used for the decomposition, steam reforming and/or partial oxidation of methane [14–20]. The H_2 production rate depends upon particle size of Ni via the dispersion and stabilization of the nickel particles by selection of an appropriate support. The reported supports so far include TiO_2, MgO, ZrO_2 and Al_2O_3 but they are reported to give relatively low H_2 production rates [17]. We find the hydroxyapatite as a support material for Ni for the CDM reaction. The compound $Ca_5(PO_4)_3(OH)$ is known as hydroxyapatite (HAp) widely used as an implant material in clinical applications owing to its biocompatibility. It finds various applications not only as a biomaterial but also as a novel support for gold and ruthenium catalysts in water gas shift reactions [21], as a catalyst for dehydrogenation and dehydration of alcohols [22] and also applied for photocatalytic applications [23, 24]. It appears that there are no reports on the use of HAp as a support material for the catalytic decomposition of methane. In this work, we report for the first time the catalytic decomposition of methane over Ni supported on HAp. The behaviour of the support material often causes the formation of traceable amounts of CO via the reaction of carbonaceous residues with lattice oxygen in the metal oxides particularly over *redox* materials during the methane decomposition reaction at high temperatures [20]. It seems true that the support materials play a critical role in determining both the methane conversion and the CO formation. Due to the non-reducible/inert nature of

IICT communication number: 051211.

J. Ashok · S. N. Kumar · M. Subrahmanyam · A. Venugopal (✉)
Catalysis & Physical Chemistry Division, Indian Institute of Chemical Technology, Hyderabad 500 007, India
e-mail: akula@iict.res.in

hydroxyapatite, we find formation of CO is absent during CH_4 decomposition.

The results cover optimization of nickel loadings over HAp where a correlation for the CDM is observed. The catalysts were characterized using SEM, XRD, TPR, DTA, TGA, CHN analyses and Ni metal surface areas measurements by O_2 pulse chemisorption studies. The CDM activities were performed at a reaction temperature of 650 °C and atmospheric pressure.

2 Experimental

The hydroxyapatite is prepared as reported earlier in the literature [21]. In a typical method a solution of calcium nitrate tetra hydrate (Ca $(NO_3)_2{\cdot}4H_2O$) (32.6×10^{-2} mol in 200 mL water) was brought to pH 11–12 with a concentrated ammonia solution (25%) and thereafter diluted to 500 mL. Diammonium hydrogen orthophosphate of 31.8×10^{-2} mol in 300 mL of water was brought to pH 11–12 with ammonia solution and thereafter diluted to 600 mL. Under vigorous stirring the phosphate solution was added drop wise to the calcium salt over a period of 2 h to produce a milky white precipitate, subsequently boiled for 30 min, with stirring. The precipitate was washed thoroughly, filtered and dried at 100 °C overnight, calcined at 500 °C in air for 3 h to obtain hydroxyapatite $[Ca_5(PO_4)_3(OH)]$ (HAp) and the phase is confirmed by XRD analysis.

The Ni supported over HAp catalysts were prepared by a wet impregnation method in excess solution. The required amount of nickel nitrate [Ni $(NO_3)_2{\cdot}6H_2O$] was taken to give Ni loadings of 5, 10, 15, 20, 30, 40, 50, 60 and 70 (wt%) over HAp. The solutions were dried with constant stirring at 100 °C until the sample gets dried and kept for oven drying at 100 °C for a duration of 12 h and subsequently calcined in static air at 700 °C. For convenience catalysts were denoted with Ni (wt%) and are *reported* in Table 1.

The DTA and TG analysis of samples were recorded using Leeds and Northup (USA) unit at a heating rate of 10 °C/min ranging from 20 to 1,000 °C under nitrogen flow [25]. The morphology of the fresh and used catalysts is analyzed with scanning electron microscopy (SEM) of JEOL-JSM 5600 instrument. XRD patterns of the samples were obtained on a Rigaku miniflex X-ray diffractometer using Ni filtered Cu K_α radiation at $2\theta = 2$–$80°$ with a scanning rate of $2°\text{min}^{-1}$ and the beam voltage and currents of 30 kV and 15 mA, respectively. The nickel particle size is estimated using Scherrer equation, $L = 0.89\lambda/\beta\cos\theta$ where, L = average particle size, λ = wavelength of Cu K_α radiation (0.154 nm), β = half-height width of diffraction peaks and θ = Bragg angle [26].

Temperature programmed reduction (TPR) and O_2 pulse chemisorption for Ni metal area analyses were carried out using a pulse micro reactor interfaced to gas chromatograph (GC) with thermal conductivity detector (TCD) unit. For subjecting TPR analysis the catalyst sample of about 50 mg was loaded in an isothermal zone of the reactor and degassed at a ramping rate of 10 °C/min up to 450 °C in helium flow. The sample was cooled to room temperature and the helium gas is replaced by 5% H_2 in Ar at a flow rate of 30 cc/min and the temperature is increased to 700 °C with a ramping rate of 5 °C/min. The reactor effluent gas is passed through a molecular sieve trap (to remove the produced water). The H_2 uptakes were measured by GC with TCD [27]. Once the TPR study is completed, the sample was cooled to 430 °C in He stream and flushed for 30 min. The oxygen uptakes were measured using pulse chemisorption of 5% O_2/He gas mixture. The O_2 uptakes and the Ni metal surface areas were calculated with respect to NiO phase [28, 29]. The carbon contents were measured using VARIO EL, CHNS analyser.

Table 1 Summary of the data obtained over Ni/HAp catalysts at temperature 650 °C

Ni (wt%)	Size of Ni (nm)[a]	Hydrogen yield (mmol/g-cat)[b]	Carbon yield (mmol/g-cat)[c]	O_2 uptake (μmol/g-cat)[d]	Ni metal area × 10^2 (m^2/g)
0[e]	–	–	–	–	–
5	18	94.6	48.2	2.715	29
10	19	118.2	61.5	3.036	32
15	20	125.1	63.6	3.230	34
20	22	247.2	124.1	3.775	40
30	24	549.1	273.9	6.224	66
40	25	478.7	238.8	5.955	63
50	28	366.9	186.2	5.728	61
60	30	338.2	172.5	5.155	55
70	35	279.5	142.1	4.575	48

[a] From XRD analysis

[b] From GC analysis

[c] By CHNS analysis

[d] Pulse O_2 chemisorption at temperature 430 °C

[e] Bare hydroxyapatite (HAp)

The CDM activities of Ni/HAp samples were performed at 650 °C at atmospheric pressure at a space velocity of 24,000 mL/h g-cat in a fixed-bed vertical quartz reactor (i.d. = 10 mm, length = 46 cm) operated in down flow mode. Powdered catalyst samples (200 mg) were held with a quartz wool bed. Prior to the reaction catalyst is reduced at 450 °C with 5% H_2 in N_2 for 2 h. The pre catalytic zone of the reactor is maintained at 200 °C. The CDM reaction is continued at 650 °C until the catalyst is completely deactivated. The concentrations of hydrogen and methane were determined using calibrated data to obtain methane conversions (number of moles of methane converted divided by number of moles of methane fed). The analysis begins at 5 min after methane gas passed over the catalyst. The reaction is continued until the CH_4 conversion is negligible and it indicates that the catalyst is completely deactivated and further no more conversions are possible. The carbon contents over the catalysts are monitored taking methane conversions during the course of the reaction also by CHNS analysis as well as gain in weight after the CDM reaction by measuring the weight of deactivated catalysts. The quantification of carbon estimations found to be more or less equal and the error bar is ±2% unless otherwise mentioned.

3 Results and Discussion

3.1 Ni/HAp for Methane Decomposition

Catalytic activity runs were performed in a fixed bed micro-reactor over 5–70 wt% Ni/HAp catalysts. The experiments were performed under similar reaction conditions in order to detect the influence of Ni loading. Figure 1 represents the change in methane conversion with time on stream. The reaction is continued until the CH_4 conversion of about 2–3%. At this stage the reaction is stopped and the catalyst sample is recovered assuming that the catalyst is deactivated. It is interesting to see that the 30 wt% Ni/HAp catalyst found to have high CH_4 decomposition activity and longevity compared to other catalysts. The pure support material, i.e. $Ca_5(PO_4)_3(OH)$ (HAp) do not show any CH_4 decomposition activity (Table 1). It appears that the HAp is acting as a good dispersing agent for Ni for CDM process. The H_2 production rates (Fig. 2) are increased with increase in Ni loading up to 30 wt% and gradually decreased up to 70 wt%. The product analysis evidences H_2 formation and no by products are seen as given in the reaction below.

$$CH_4 \rightarrow C + 2H_2 \quad \Delta H^\circ = 75.6\,\text{kJ/mole}$$

Thus suggests the hydroxyapatite is one of the suitable supports for CDM reaction for the production of pure hydrogen applied in fuel cell technology. The high carbon to nickel ratio corroborates the sustainability and longevity of 30 wt% Ni sample compared to other compositions. The methane conversion is generally found to be high at initial stages and it decreases (for some time) due to carbon deposition with time on stream thus deactivate the catalyst finally. The accumulated carbon on the surface of the catalyst, cover/block the active sites eventually cause pore-mouth plugging. This is noticed from XRD analysis and the carbon estimations performed for deactivated samples recovered after the reaction. The performance of supported Ni catalysts for CH_4 decomposition strongly depends upon the metal-support interaction, Ni loading and also the particle size [8].

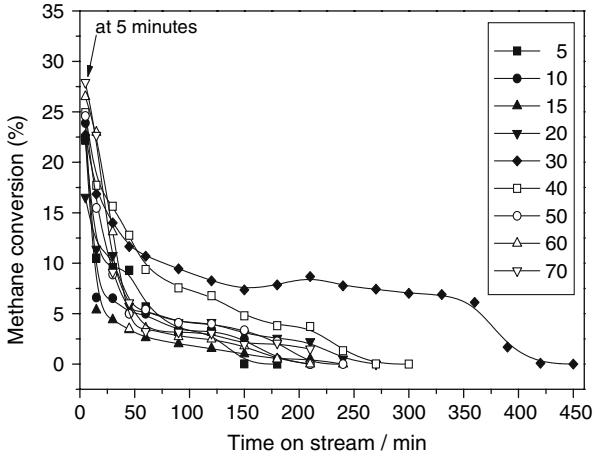

Fig. 1 Methane conversion over Ni (wt%) supported HAp. Temperature = 650 °C, atmospheric pressure

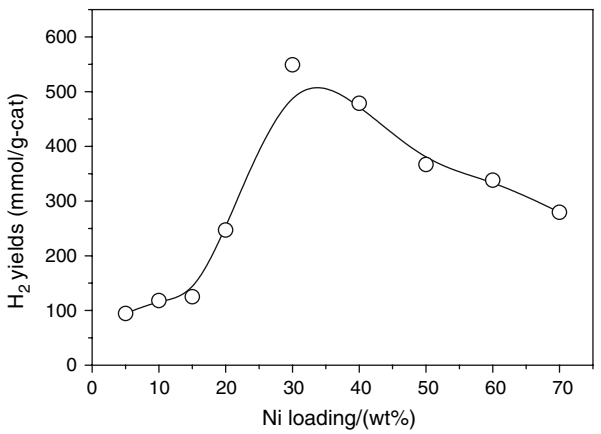

Fig. 2 Hydrogen yields during methane decomposition as a function of Ni loading over Ni/HAp catalysts

In the present investigation, a maximum of 550 mmol H_2/g-cat is observed over 30 wt% Ni/HAp catalyst. This enhances the scope for exploring further investigation of hydroxyapatite as a support material with different active metal components for catalytic reforming and cracking of hydrocarbons and alcohols.

3.2 XRD Analysis

The XRD patterns of fresh Ni/HAp samples are displayed in Fig. 3. The reflections at $2\theta = 37.28°$, 43.3°, 62.9° with corresponding d values of 0.209, 0.148, 0.241 nm are attributed to the presence of crystalline NiO phase [ICSD No: 01-1239]. The diffraction lines at $2\theta = 25.8°$, 29.1°, 31.9°, 33.1°, 32.2°, 34.1°, 40.1°, 46.9°, 49.1° and their corresponding d values 0.344, 0.306, 0.279, 0.277, 0.269, 0.262, 0.224, 0.193, 0.183 nm [ICSD No: 86-0740] is attributed to the presence of crystalline $Ca_5(PO_4)_3(OH)$ (hydroxyapatite) phase [21]. It is clearly seen from XRD patterns that the intensity of NiO phase is increased with Ni content. The NiO in fresh catalysts suggests the decomposition of nickel nitrate in air at 700 °C for 5 h, resulting the formation of NiO species during the preparation and calcination.

The XRD patterns of deactivated catalysts are shown in Fig. 4. The amount of carbon depends upon the activity and longevity of the specific catalyst. The irreversible carbon deposited on the samples is evident from XRD patterns of the deactivated. The diffraction lines at $2\theta = 26.28°$, 45.2°, 53.9°, 77.0° and their corresponding d values of 0.338, 0.2, 0.169, 0.123 nm are attributed to graphitic nature of carbon [ICSD NO: 01-0640] which is evidenced over all the deactivated catalysts. The metallic Ni phase and its reflections at $2\theta = 44.4°$, 51.8°, 76.4° and the corresponding d values of 0.203, 0.176, 0.124 nm is observed in all the deactivated catalysts [ICSD No: 04-0850]. Presence of metallic Ni in the deactivated catalysts indicates the NiO phase is reduced to metallic Ni during the course of reduction and reaction. It appears that the metallic nickel is active for the decomposition of methane. The increase in amount of deposited carbon is seen with increase in relative peak intensity of the graphitic carbon at $2\theta = 26.28°$ from the XRD patterns of deactivated catalysts. The crystallite size of Ni measured by XRD analysis of the Ni/HAp catalysts are found to be 18–35 nm and reported *in* Table 1. The average particle size increased gradually with increase of Ni loadings. It is observed that the Ni particles of ~24 nm are having larger C/Ni ratio where the Ni loading seems to be optimum over HAp for

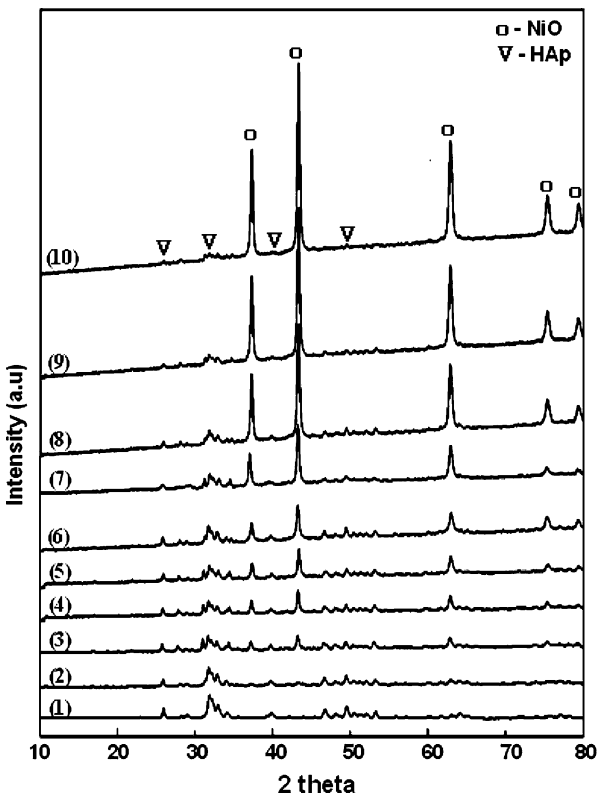

Fig. 3 XRD patterns of fresh Ni (wt%) 1, 0; 2, 5; 3, 10; 4, 15; 5, 20; 6, 30; 7, 40; 8, 50; 9, 60; and 10, 70 supported on HAp

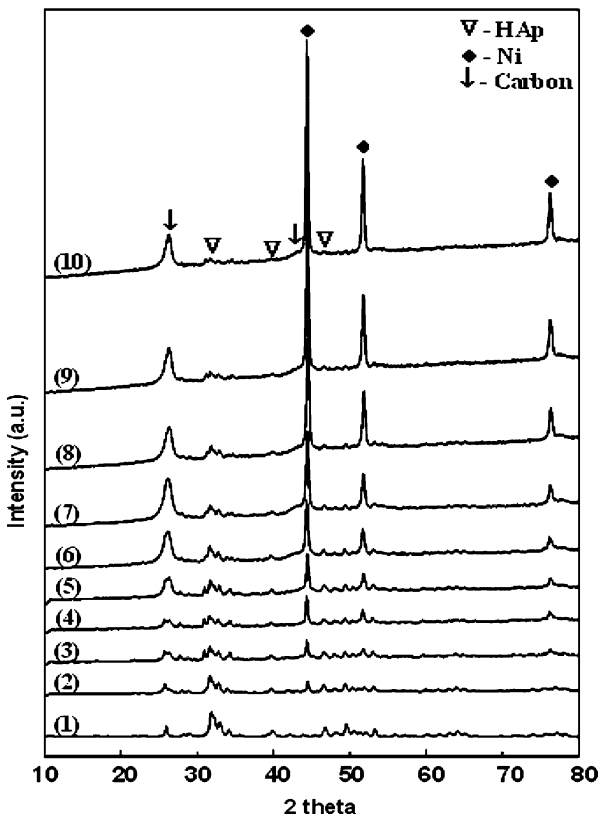

Fig. 4 XRD patterns of used Ni (wt%) 1, 0; 2, 5; 3, 10; 4, 15; 5, 20; 6, 30; 7, 40; 8, 50; 9, 60; and 10, 70 supported on HAp

CDM process. Finally it can be concluded that the fresh catalyst contains both NiO and $Ca_5(PO_4)_3(OH)$ (HAp) phases and the deactivated samples pose due to metallic Ni, graphitic carbon in major and HAp peaks with minor intensities.

3.3 TGA and DTA

The TG and DTA graphs of Ni over HAp catalysts are shown in Figs. 5 and 6, respectively. The TG analysis (Fig. 5) revealed that there is a gradual weight loss and is proportional with nickel content up to 500 °C and above this point it levels off up to 1,000 °C. The decomposition of nickel nitrate to NiO is a complex multi step solid-state reaction and many of the steps that could affect the support material for nucleation site density and NiO crystal growth rate [30, 31]. The DTA profiles of Ni loaded HAp showed (Fig. 6) the occurrence of endothermic changes at five temperatures (°C) falls between, 100–120; 178–200; 250–260; 290–390 and 450–460 [14]. The first two peaks are probably due to the release of physisorbed and structural water whereas the other three endothermic peaks correspond to phase transitions occurred for nickel nitrate. The

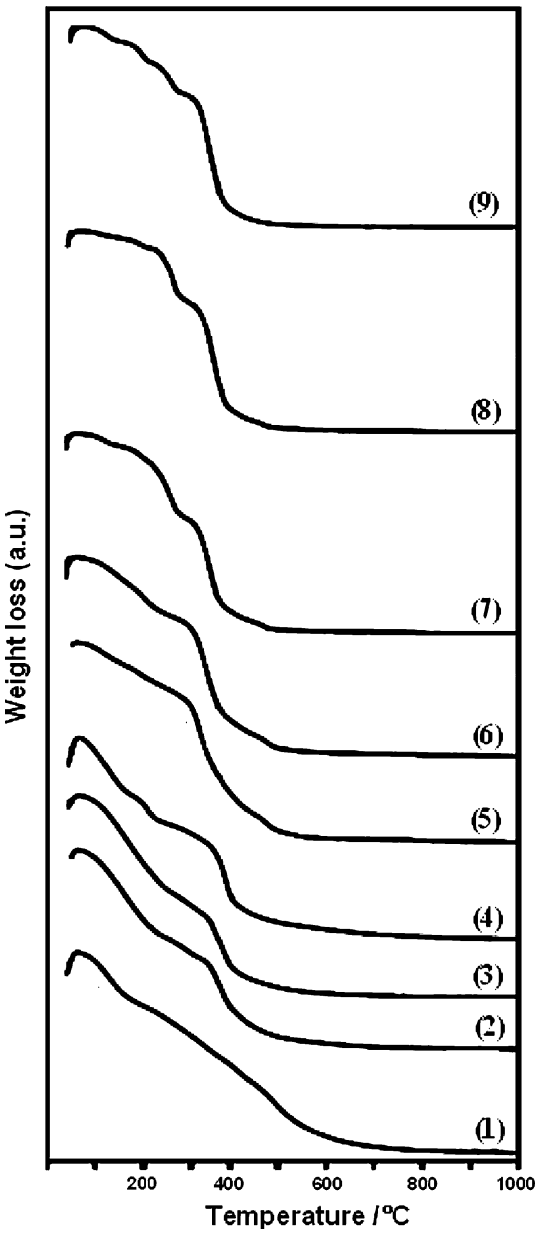

Fig. 5 TGA of oven dried Ni (wt%) 1, 5; 2, 10; 3, 15; 4, 20; 5, 30; 6, 40; 7, 50; 8, 60; 9, 70 over HAp support

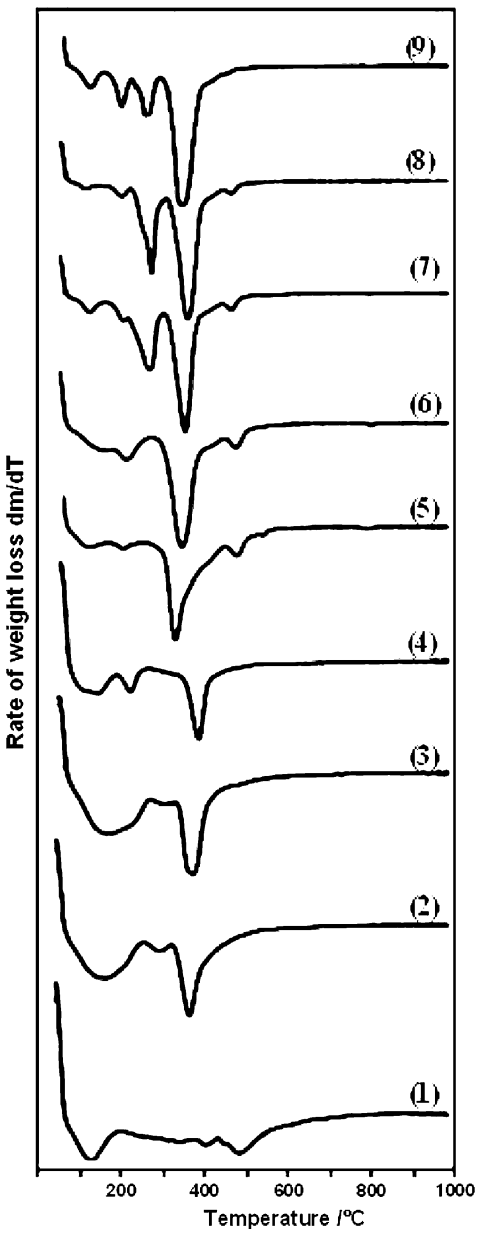

Fig. 6 DTA of oven dried Ni (wt%) 1, 5; 2, 10; 3, 15; 4, 20; 5, 30; 6, 40; 7, 50; 8, 60; 9, 70 over HAp support

formation of NiO phase in calcined form of the catalyst is confirmed by XRD analysis. The DTA analysis revealed that all the thermal transitions are taking place below 460 °C and no endothermic peak is observed above 460 °C. This clearly suggests that hydroxyapatite is stable even at high temperatures as no possible thermal transitions that were observed in this study. Thermal stability of the active component and the support material is a key factor particularly when applied for high temperature hydrocarbon reforming and cracking reactions.

3.4 Temperature Programmed Reduction

Figure 7 shows the typical TPR profiles of 5–70 wt% Ni/HAp catalysts. The XRD analysis of fresh catalysts revealed the presence of NiO phase. The quantification of H_2 consumption is estimated using Cu_2O as standard sample for TPR analysis. TPR patterns (Fig. 7) indicated that increase in Ni loading the H_2 uptakes are increased. The T_{max} is found to be around ca. 430 °C in all the case. The pure $Ca_5(PO_4)_3(OH)$ do not show any reduction signals even up to 700 °C indicating the characteristic non-reducible behaviour of hydroxyapatite material [21]. The TPR of reference NiO (bulk) is performed for comparison purpose and the T_{max} is centered at 443 °C. All the samples 5–70 wt% Ni/HAp exhibited the reduction maxima, i.e. T_{max} (°C) between $400 < (T_{max}) < 500$. It is evident that bulk NiO species is present in all the fresh calcined samples.

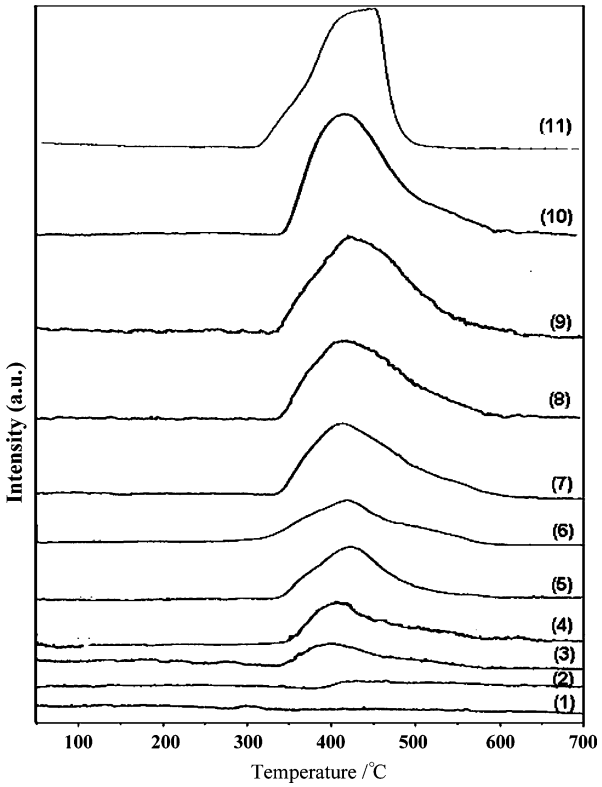

Fig. 7 TPR profiles of Ni (wt%) 1, 0; 2, 5; 3, 10; 4, 15; 5, 20; 6, 30; 7, 40; 8, 50; 9, 60; 10, 70 over HAp catalysts and 11, bulk NiO

3.5 O_2 Pulse Chemisorption

The O_2 pulse chemisorption over Ni/HAp catalysts is performed and the Ni metal surface area are measured and reported in Table 1. The O_2 uptakes are increased with Ni loading up to 30 wt% and above this loading gradually decreased up to 70 wt%. Thus suggesting high Ni surface coverage over 30 wt% Ni/HAp compared to other compositions. The better performance of 30 wt% Ni/HAp is noteworthy due to the presence of number of effective Ni particles assisting the growth of carbon nanofibers and thereby high H_2 production rates. A linear relation between the Ni metal surface area and the H_2 yields are shown in Fig. 8. In view of this it is concluded that 30 wt% is an optimum composition in case for Ni supported over HAp catalysts.

3.6 Carbon Analysis (CHNS)

The decomposition of methane is performed under similar reaction conditions for all the samples. The deactivation is apparently due to carbon deposition and is seen by the increase in weight of the catalysts after reaction. Furthermore, the deactivated catalysts are recovered in an inert gas atmosphere and subsequently estimated for carbon deposits. It is evident from CHN analysis data of the deactivated samples that carbon contents gradually increased until 30 wt% Ni and decreased with Ni loading up to 70 wt%. The XRD analysis of the deactivated catalysts supports the

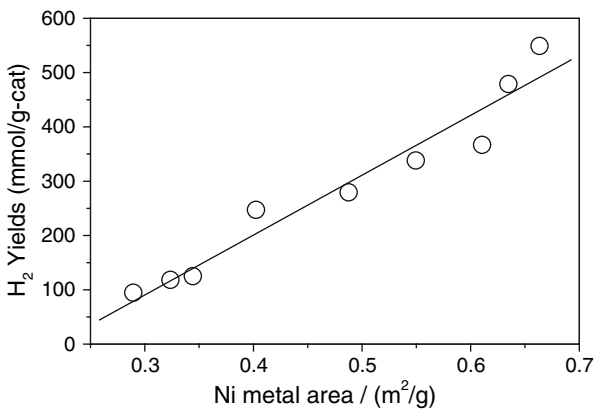

Fig. 8 Hydrogen production as a function Ni metal surface area

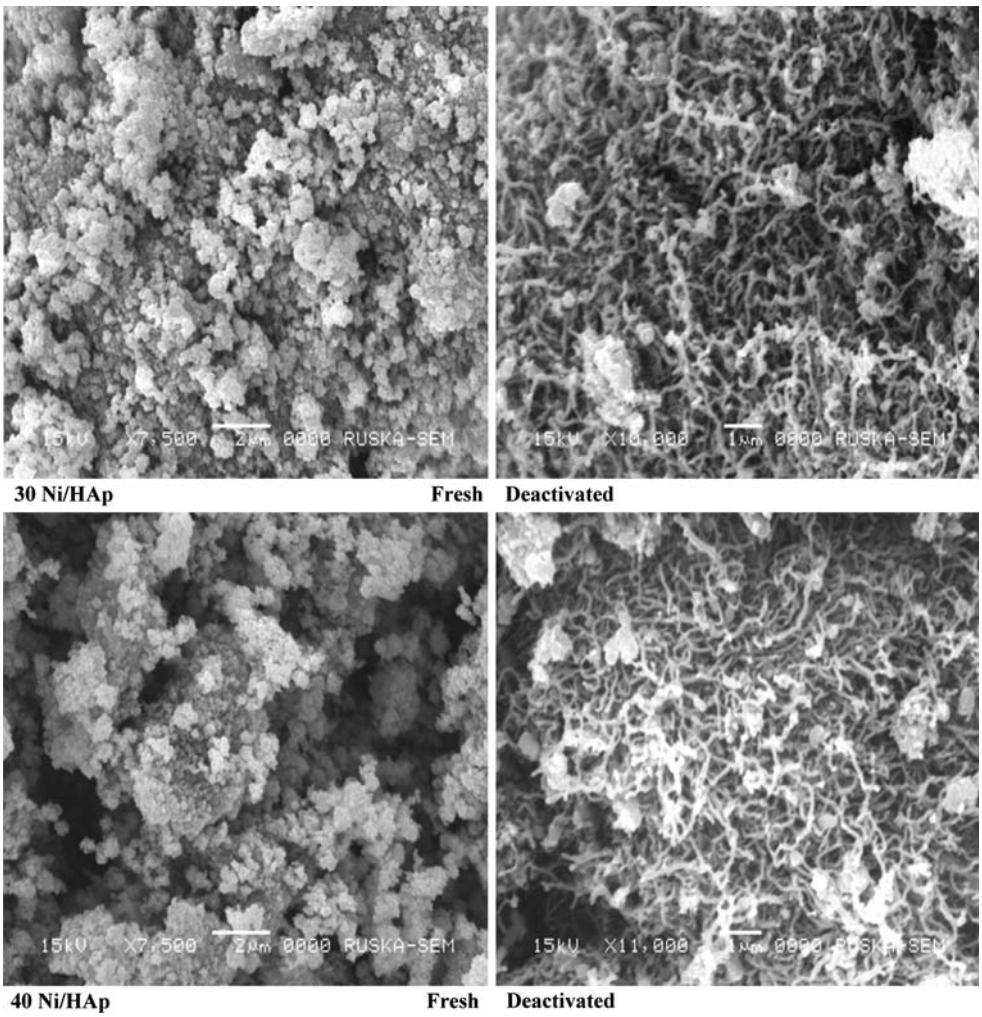

Fig. 9 The SEM images of fresh and deactivated 30, 40 wt% Ni/HAp catalysts

finding of graphitic carbon in deactivated catalyst. In general, the CDM activity and longevity of the Ni based catalysts are correlated with the extent of carbon deposition and it is found to be irreversible under the present reaction conditions over Ni/HAp catalysts. The irreversible nature of graphitic carbon is further confirmed by TPR analysis of the deactivated catalysts that could not display any reduction profiles due to hydrogasification, i.e. absence of hydrogenation of carbon to hydrocarbon even at 700 °C.

3.7 SEM Analysis

The SEM micrographs of fresh and deactivated catalysts of 30 and 40 wt% Ni samples are displayed in Fig. 9. Formation of graphitic carbon filaments with relatively uniform diameters is evident from SEM analysis. Micrographs of both the 30 and 40 wt% deactivated catalysts showed the surface is completely covered with filamentous carbon in contrast to clean surfaces of the fresh samples. The shiny patches in the deactivated catalysts are probably due to Ni particle occupied at the tip of the carbon nanofibers. Similar observations are reported during catalytic decomposition of methane over supported Ni catalysts [7–9].

4 Conclusions

The XRD patterns of deactivated catalysts showed reflections due to metallic Ni, graphitic carbon in major intensities, which is clearly visualized from the SEM analysis. The hydroxyapatite phase is intact even after exposing it to CH_4 at 650 °C for a long period. The 30 wt% Ni over HAp catalyst demonstrated high CH_4 decomposition activity and longevity when compared to other compositions. The O_2 pulse chemisorption studies revealed high Ni metal surface area over 30 wt% Ni/HAp catalyst, could be *a* reason why higher CDM activity than the other catalysts. It is observed that hydroxyapatite is found to be one of the stable and useful support/dispersing agents for Ni during methane decomposition reaction. This enhances

the scope for exploring further investigation of hydroxyapatite as a support material with different active metal components for high temperature catalytic cracking of hydrocarbons and reforming alcohols for the production of hydrogen.

Acknowledgment The authors thank CSIR, New Delhi for funding this project under NMITLI program.

References

1. Thomas CE, James BD, Lomax FD, Kuhn IF (1998) Int J Hydrogen Energy 25:551
2. De Jong KP, Geus JW (2000) Catal Rev Sci Eng 42:481
3. Ebbesen TW (1997) Carbon nanotubes: preparation and properties. CAPLUS, USA
4. Bahome MC, Jewell LL, Hildebrandt D, Glasser D, Coville NJ (2005) Appl Catal A 287:60
5. Serp P, Corrias M, Kalck P (2003) Appl Catal A 253:337
6. Chambers A, Park C, Baker RTK, Rodriguez NM (1998) J Phys Chem B 102:4253
7. Ashok J, Naveen Kumar S, Venugopal A, Durga Kumari V, Subrahmanyam M (2007) J Power Sources 164:809
8. Ashok J, Naveen Kumar S, Subrahmanyam M, Venugopal A (2007) Catal Lett 118:139
9. Venugopal A, Naveen Kumar S, Ashok J, Hari Prasad D, Durga Kumari V, Prasad KBS, Subrahmanyam M (2007) Int J Hydrogen Energy 32:1782
10. Ashok J, Naveen Kumar S, Venugopal A, Tripathi S, Durga Kumari V, Subrahmanyam M (2007) Catal Commun 9:164
11. Serban M, Lewis MA, Marshall CL, Doctor RD (2003) Energy Fuels 17:705
12. Muradov N (1998) Energy Fuels 12:41
13. Choudhary TV, Aksoylu E, Goodman DW (2003) Catal Rev 45:151
14. Takenaka S, Shigeta Y, Tanabe E, Otsuka K (2003) J Catal 220:468
15. Ermakova MA, Ermakova DY, Kuvshinov GG, Plyasova LM (1999) J Catal 187:77
16. Shaikhutdinov SK, Avdeeva LB, Novgorodov BN, Zaikovskii VI, Kochubey DI (1997) Catal Lett 47:35
17. Li J, Lu G, Li K, Wang W (2004) J Mol Catal A 221:105
18. Avdeeva LB, Goncharova OV, Kochubey DI, Zaikovskii VI, Plyasova LM, Novgorodov BN, Shaikhutdinov SK (1996) Appl Catal A 141:117
19. Reshetenko TV, Avdeeva LB, Ismagilov ZR, Chuvilin AL, Ushakov VA (2003) Appl Catal A 247:51
20. Choudhary TV, Sivadinarayana C, Chusuei CC, Klinghoffer A, Goodman DW (2001) J Catal 199:9
21. Venugopal A, Scurrell MS. (2003) Appl Catal A: 245:137
22. Bett JAS, Christner LG, Hall WK (1967) J Am Chem Soc 89:5535
23. Pratap Reddy M, Venugopal A, Subrahmanyam M (2007) Water Res 41:379
24. Pratap Reddy M, Venugopal A, Subrahmanyam M (2006) Appl Catal B 69:164
25. Otsuka K, Takenaka S (2004) Appl Catal A 273:113
26. Bond GC (1987) Heterogeneous catalysis: principles and applications. Oxford University Press, New York, p 81
27. Muradov NZ (1993) Int J Hydrogen Energy 18:211
28. Poncelet G, Centeno MA, Molina R (2005) Appl Catal A 288:232
29. Stytsenko VD (1995) Appl Catal A 126:1
30. Ishihara T, Miyashita Y, Iseda H, Takita Y (1995) Chem Lett 24:93
31. Delannay F, Delmon B (1984) In: Delannay F (ed) Characterization of heterogeneous catalysts, Marcel Dekker Inc., New York, p 1
32. Mile B, Stirling D, Zammitt MA, Lovell A, Webb M (1988) J Catal 114:217